Supporting Information

# A new family of anti-perovskite oxyhydrides with tetrahedral $GaO_4$ polyanions

Nur Ika Puji Ayu,[a,b] Fumitaka Takeiri,*[b,c,d,e] Takafumi Ogawa,[f] Akihide Kuwabara,[f] Masato Hagihala,[a,b] Takashi Saito,[a,b] Takashi Kamiyama,[a,b,g,h] and Genki Kobayashi*[b,c,e]

*Corresponding author

fumitaka.takeiri@riken.jp (Fumitaka Takeiri), genki.kobayashi@riken.jp (Genki Kobayashi)

[a] *Neutron Science Laboratory (KENS), Institute of Materials Structure Science, High Energy Accelerator Research Organization (KEK), 203-1 Shirakata, Tokai, Ibaraki 319-1106, Japan*

[b] *SOKENDAI (The Graduate University for Advanced Studies), Shonan Village, Hayama, Kanagawa 240-0193, Japan*

[c] *Department of Materials Molecular Science, Institute for Molecular Science, 38 Nishigonaka, Myodaiji, Okazaki, Aichi 444-8585, Japan*

[d] *PRESTO, Japan Science and Technology Agency (JST), Kawaguchi, Saitama 332-0012, Japan*

[e] *Solid State Chemistry Laboratory, Cluster for Pioneering Research (CPR), RIKEN, Wako 351-0198, Japan*

[f] *Nanostructures Research Laboratory, Japan Fine Ceramics Center, 2-4-1 Mutsuno, Atsuta-ku, Nagoya, 456-8587, Japan*

[g] *Institute of High Energy Physics, Chinese Academy of Sciences, Beijing, 100049, China*

[h] *China Spallation neutron source science center, Dongguan, 523803, China*

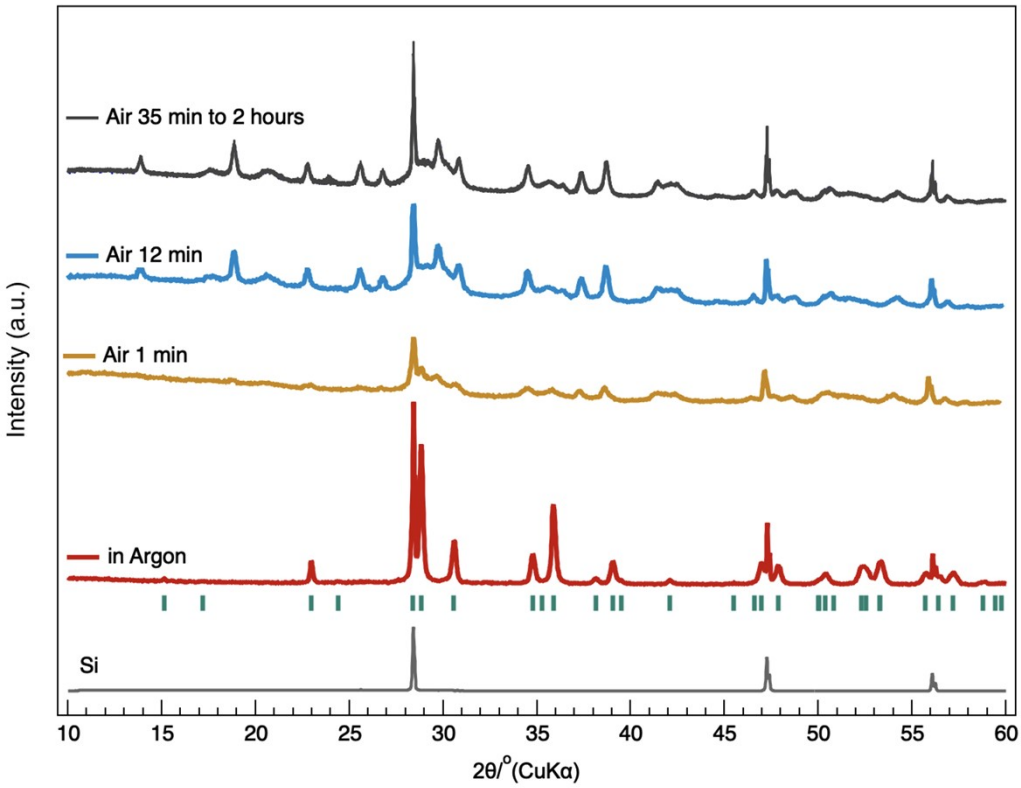


**Figure S1.** Stability of $Ba_{3-x}GaO_4H_{1-y}$ in air checked by laboratory XRD. Silicon powder (light gray line) was added as a reference of the peak position. The red line represents the pattern of as-prepared product measured in an Ar-filled sample holder. The yellow, blue, and dark gray lines represent the patterns measured in air after 1, 12 and $\geq$ 35 minutes.

**Table S1(a)** Refined crystal structure parameters from SXRD data of $Ba_{3-x}GaO_4H_{1-y}$

| atom | site | *g* | *x* | *y* | *z* | *B* / Å² |
|---|---|---|---|---|---|---|
| Ba1 | 4*a* | 0.92916(6) | 0 | 0 | 1/4 | 1.333(8) |
| Ba2 | 8*h* | 1 | 0.17327(2) | 0.67315(2) | 0 | 0.547(5) |
| Ga | 4*b* | 1 | 0 | 1/2 | 1/4 | 0.626(11) |
| O1 | 16*l* | 1 | 0.1487(2) | 0.6487(2) | 0.6520(1) | 2.50(4) |

Unit cell: *I*4/*mcm*; $a = b = 7.29616(3)$ Å, $c = 11.70656(6)$ Å,
$S = 2.48$, $R_{wp} = 7.49\%$, $R_p = 5.21\%$, $R_e = 3.02\%$, $R_B = 4.34\%$, $R_F = 3.27\%$.

**Table S1(b)** Refined crystal structure parameters from SXRD data of $Sr_{3-x}GaO_4H_{1-y}$

Phase 1: $Sr_{3-x}GaO_4H_{1-y}$ (82.3 wt%)

| atom | site | *g* | *x* | *y* | *z* | *B* / Å² |
|---|---|---|---|---|---|---|
| Sr1 | 4*a* | 0.9219(5) | 0 | 0 | 1/4 | 0.892(11) |
| Sr2 | 8*h* | 1 | 0.17310(3) | 0.67310(3) | 0 | 0.130(7) |
| Ga | 4*b* | 1 | 0 | 1/2 | 1/4 | 0.389(10) |
| O1 | 16*l* | 1 | 0.15529(8) | 0.65529(8) | 0.64920(6) | 1.86(2) |

Unit cell: *I*4/*mcm*; $a = b = 6.901414(5)$ Å, $c = 11.341604(10)$Å,

$S = 6.82$, $R_{wp} = 5.98\%$, $R_p = 3.98\%$, $R_e = 0.88\%$, $R_B = 5.31\%$, $R_F = 3.24\%$.

Phase 2: SrO (17.7% wt%)

| atom | site | *g* | *x* | *y* | *z* | *B* / Å² |
|---|---|---|---|---|---|---|
| Sr1 | 4*b* | 1 | 1/2 | 1/2 | 1/2 | 0.29 |
| O1 | 4*a* | 1 | 0 | 0 | 0 | 0.34 |

Unit cell: *Fm*-3*m*; $a = 5.157548(2)$, $R_B = 3.42\%$, $R_F = 2.01\%$.

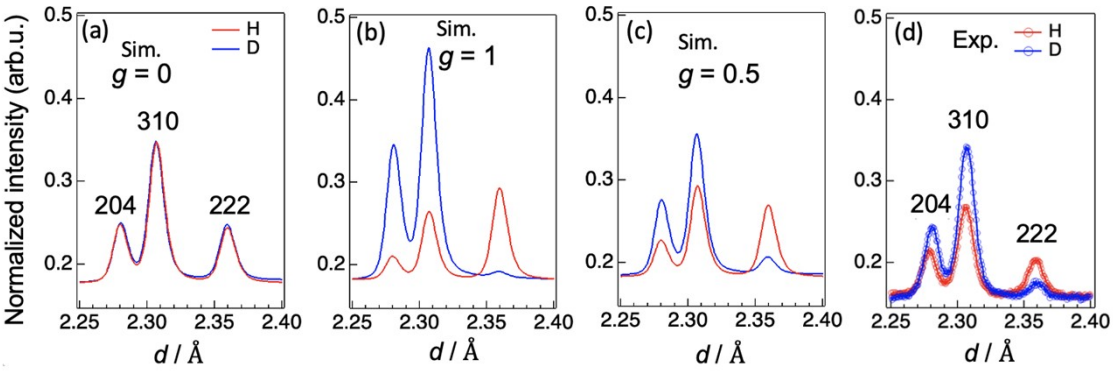


**Figure S2.** The calculated neutron diffraction patterns of 204, 310, 222 peaks of $Ba_{2.85}GaO_4H_{1-y}$ (red) and $Ba_{2.85}GaO_4D_{1-y}$ (blue) varying on H/D occupancy ($g$) for (a) $g$(H/D) = 0 ($y$ = 1), (b) $g$(H/D) = 1 ($y$ = 0), and (c) $g$(H/D) = 0.5 ($y$ = 0.5), compared to (d) its experimental data, respectively.

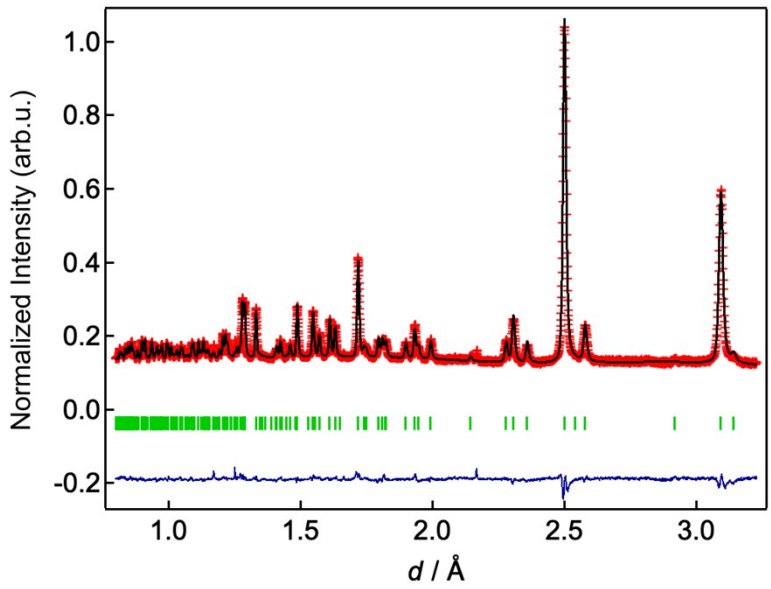


**Figure S3.** Refined Neutron diffraction (ND) pattern of $Ba_3GaO_4H$ at 300 K. The red, black, and blue lines represent observed intensity, calculated intensity, and their difference, respectively. The green marks represent the peak position of $Ba_3GaO_4H$.

**Table S2.** Refined structural parameters determined by the ND pattern of $Ba_{2.8}GaO_4H_{0.7}$ at 300 K

| Atom | Site | *g* | *x* | *y* | *z* | *B* / Å² |
|---|---|---|---|---|---|---|
| Ba1 | 4*a* | 0.801(3) | 0 | 0 | 1/4 | 0.73(2) |
| Ba2 | 8*h* | 1 | 0.17304(6) | 0.67304(6) | 0 | 0.492(13) |
| Ga1 | 4*b* | 1 | 0 | 1/2 | 1/4 | 0.494(15) |
| H1 | 4*c* | 0.699(3) | 0 | 0 | 0 | 0.61(3) |
| O1 | 16*l* | 1 | 0.14015(4) | 0.64015(4) | 0.65054(3) | 0.675(9) |

Unit cell: *I*4/*mcm*; $a$ = 7.29363(4) Å, $c$ = 11.68046(10) Å

$S$ = 4.04, $R_{wp}$ = 3.94%, $R_p$ = 12.69%, $R_e$ = 0.98%, $R_B$= 13.08%, $R_F$= 12.82%.

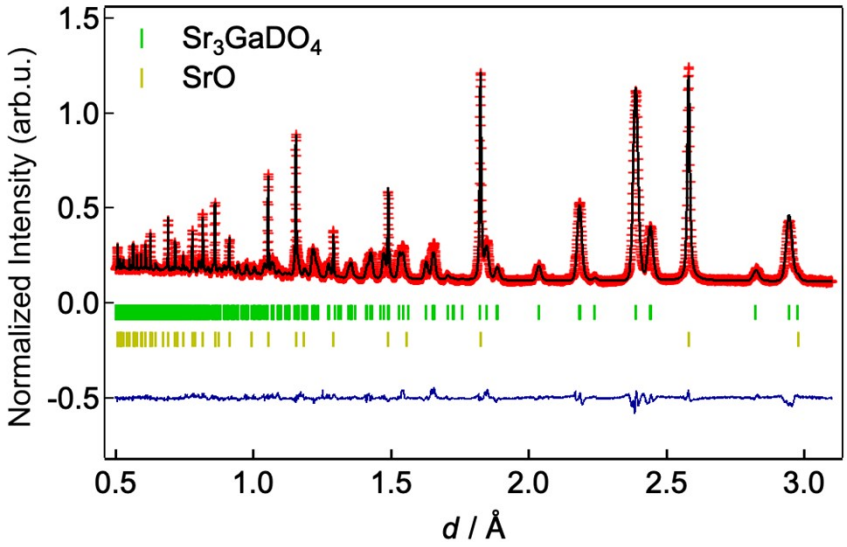


**Figure S4.** Refined Neutron diffraction (ND) pattern of $Sr_3GaO_4D$ at 300 K. The red, black, and blue lines represent observed intensity, calculated intensity, and their difference, respectively. The green and yellow marks represent the peak position of $Sr_3GaO_4D$ and SrO, respectively.

**Table S3.** Refined structural parameters determined by the ND pattern of $Sr_3GaO_4D$ at 300 K

Phase 1: $Sr_{2.933}GaO_4D_{0.762}$ (67.14 wt%)

| Atom | Site | *g* | *x* | *y* | *z* | *B* / Å² |
|---|---|---|---|---|---|---|
| Sr1 | 4*aa* | 0.933(2) | 0 | 0 | 1/4 | 1.53(2) |
| Sr2 | 8*h* | 1 | 0.17327(4) | 0.67327(4) | 0 | 0.20(2) |
| Sr1 | 4*b* | 1 | 0 | 1/2 | 1/4 | 0.19(1) |
| D1 | 4*c* | 0.762(2) | 0 | 0 | 0 | 2.12(3) |
| O2 | 4*c* | 1 | 0.14394(4) | 0.64394(4) | 0.64588(4) | 1.59(1) |

Unit cell: *I*4/*mcm*, $a$ = 6.89849(4) Å, $c$ = 11.29481(13) Å.

$S$ = 3.98, $R_{wp}$ = 4.23%, $R_p$ = 2.99%, $R_B$ = 7.74%, $R_F$ = 6.89%.

Phase 2: SrO (32.86 wt%)

| Atom | Site | *g* | *x* | *y* | *z* | *B* / Å² |
|---|---|---|---|---|---|---|
| Sr | 4*a* | 1 | 1/2 | 1/2 | 1/2 | 0.433 |
| O | 4*b* | 1 | 0 | 0 | 0 | 0.523 |

Unit cell: *Fm*−3*m*, $a$ = 5.158078(6) Å; $R_B$ = 3.19%, $R_F$ = 3.04%.

**Pont-defect calculations**

In order to investigate the behavior of point defects in the $Ba_3GaO_4H$ crystal, we examined the formation energies and related densities of isolated point defects in the crystal. Here, we consider point defects relating to Ba and H atoms, and Ga and O atoms occupy the crystal site without any defects, based on the Rietveld-analysis results.

Point-defect calculations of $Ba_3GaO_4H$ were performed using 2 × 2 × 1 supercell and 1 × 1 × 2 ***k***-point grid. The defect formation energies are evaluated following the conventional definition shown elsewhere.[1] For defects with a non-zero charge state, the FNV-correction[2, 3] was adopted using the calculated dielectric functions: $e_{xx} = e_{yy} = 24.91$ (= 4.23 + 20.68) and $e_{zz} = 17.80$ ( = 4.25+13.55), where values in the parentheses indicate the contributions from electronic and ionic parts, respectively. In this work, the chemical potential of Ba atoms was determined to reproduce the composition $Ba_{2.85}GaO_4H_{1\pm\delta}$ obtained experimentally, while that of H atoms was by $H_2$-gas pressure. The Fermi level was determined to maintain the charge neutrality condition and temperature was set to be 1000 K. This type of calculations can be performed via recently developed constant-*N* approach for point defect thermodynamics, as implemented in the pydecs code (https://gitlab.com/tkog/pydecs).

Figure S5(a) and S5(b) shows calculated defect formation energies and defect concentrations, respectively. In Fig. S5(b), electrons and holes are not presented because of its' tiny amounts. This indicates the electronic carriers are hardly produced due to the wide band gap. As a general trend, Ba vacancies equilibrate with interstitial H atoms and H vacancies at relatively higher and lower pressure, respectively. The latter lower-pressure situation corresponds to the Rietveld result (Table I in the main text) for the synthesized sample. Our calculations suggest the possibility that predominant H-atom defect may be adjusted via synthesis condition. For further discussion, defects of O and Ga atoms should also be considered, though these are omitted based on the experimental result in this work for simplicity of discussion.

We should note that, in the calculated results, there is an inconsistency on Ba deficiency: the energy of $V_{Ba2}^{2-}$ is lower by 0.36 eV than that of $V_{Ba1}^{2-}$, while vacancies on the Ba1 site is preferable in experiments. This contradiction suggests the importance of factors omitted in the calculations, for example, finite-temperature effect and correlation among abundant defects.

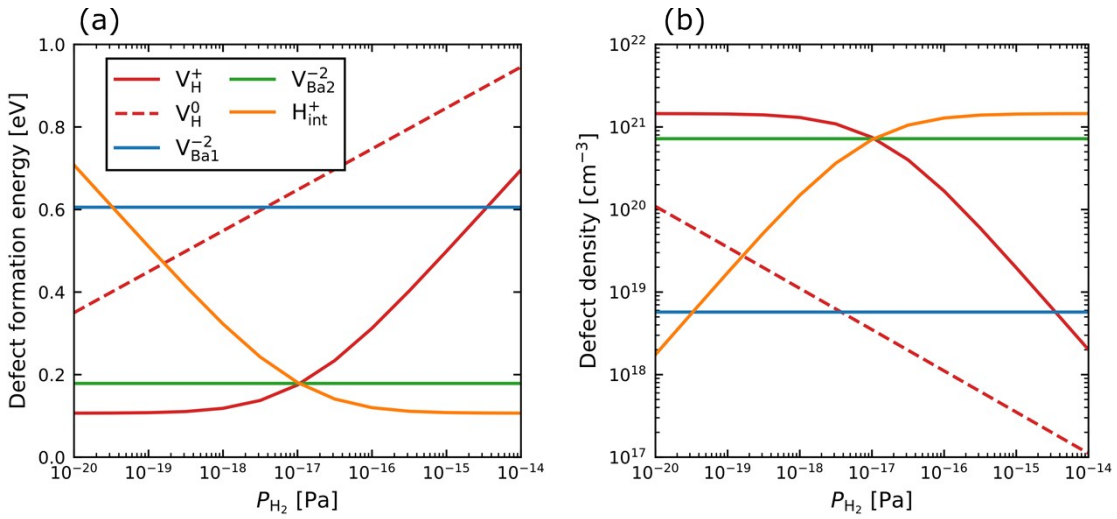


**Figure S5** (a) Defect formation energy and (b) defect densities in $Ba_3GaO_4H$, obtained by DFT calculations.

**Table S4.** Estimated Goldschmidt tolerance factors (*t*) of $A_3MO_4H$ (*A* = Ba, Sr, Ca; *M* = Al, Ga)

| Compounds | Tolerance factor *t* | Crystal structure type |
|---|---|---|
| $Sr_3GaO_4H$ | 0.948 | Tetragonal (*I*4/*mcm*) |
| $Ba_3GaO_4H$ | 0.934 | Tetragonal (*I*4/*mcm*) |
| $Sr_3AlO_4H$ [4] | 0.929 | Tetragonal (*I*4/*mcm*) |
| $Ba_3AlO_4H$ [5] | 0.916 | Orthorhombic (*Pnma*) |

The Goldschmidt tolerance factors *t* was defined as

$$t = \frac{\left(r_{MO_4} + r_A\right)}{\sqrt{2}\left(r_X + r_A\right)}$$

where $r_A$ is the cation radius in a six-coordination number, $r_X$ is the ionic radius of hydride anion that was fixed to 1.399 as suggested by Shannon,[6] and $r_{MO_4}$ is the ionic radius of $MO_4^{2-}$. The ionic radii for the determination of *t* are listed in Table S4. The values of $GaO_4^{2-}$ and $AlO_4^{2-}$ were calculated from the lattice parameters of $Sr_3GaO_4H$ (this work) and $Sr_3AlO_4H$ [4], respectively, as follows.

$$r_{MO_4} = \frac{(a - 2r_A)}{2}$$

## References:


1. C. Freysoldt, B. Grabowski, T. Hickel, J. Neugebauer, G. Kresse, A. Janotti and C. G. Van de Walle, *Reviews of Modern Physics*, 2014, **86**, 253-305.
2. C. Freysoldt, J. Neugebauer and C. G. Van de Walle, *Phys Rev Lett*, 2009, **102**, 016402.
3. Y. Kumagai and F. Oba, *Physical Review B*, 2014, **89**.
4. T. Wu, K. Fujii, T. Murakami, M. Yashima and S. Matsuishi, *Inorg Chem*, 2020, **59**, 15384-15393.
5. B. Huang and J. D. Corrbet, *Journal of Solid State Chemistry*, 1998, **141**, 570-575.
6. R. D. Shannon, *Acta Crystallography*, 1976, **A32**, 751.